1997

Boundary Layer Effect on the Frontal Interaction with Mountain

Melinda S. Peng
Naval Research Laboratory
John Powell and R. T. Williams
Naval Postgraduate School
Monterey, CA

Abstract

A hydrostatic,primitive equation model with frontogenetical deformation forcing is used to simulate the passage of cold fronts over a two-dimensional ridge. The model includes a K-theory boundary layer (PBL) parameterization with implicitly defined diffusion coefficients. Relative to the inviscid results, the PBL simulations produced reduced frontolysis on the upwind slope and reduced frontogenesis on the lee slope, resulting in significantly smaller frontogenetic variations over the mountain. This is caused by convergence forcing in the well-mixed layer offsetting the overall frontolytical forcing on the upwind slope, and greatly reduced lee side convergence forcing due to the PBL. In contrast to the inviscid results, the final downstream front is weaker in the mountain simulations than in the flat-topography control case when PBL effects are included.

1. Introduction

Mountainous topography introduces dynamical complications to meteorological phenomena on all scales, from sub-mesoscale systems to the global circulation. For example, forecasters have long known that fronts tend to weaken as they move up the windward slope of a mountain range and often intensify on the lee slope. This effect has been documented in quantitative observational studies, for example in the analyses of high-resolution Alpine Experiment (ALPEX) data of Hartsough and Blumen (1990) and Radinovic (1986). While important realistic effects can be resolved by simplified analytical treatments, the full dynamics of frontal interaction with topography are analytically intractable. Numerical simulation provides a means to investigate the dynamics of flows without analytical solutions. Important analytic and numerical studies in the past decade were reviewed in Williams et al. (1992). They perform numerical simulations to study the effect of mountain on fronts using a two-dimensional primitive equation (PE) Boussinesq model. The mountain-forced divergence weakens the front on the upwind slope and convergence on the leeside intensifies the front. The final intensity in the mountain case is similar to that of the flat topography case.

Most of previous studies consider inviscid flows only. Keyser and Anthes (1982) investigate PBL effects on frontogenesis using a two- dimensional hydrostatic PE model incorporating a mult-layer, first-order K-theory PBL parameterization. Detailed realistic frontal features not produced in inviscid simulations are evident in the PBL model results. Dunst and Rhodin (1990) obtain similar detail in their frontal simulations using a high-resolution first-order parameterization similar to the one used by Keyser and Anthes (1982), but with a different diffusion coefficient formulation.

This study seeks to improve the physical accuracy of previous numerical studies on frontal interaction with topography by including a realistic PBL parameterization. The basic model is the two-dimensional Boussinesq PE model of Williams et al. (1992, denoted W92) with the inclusion of a first order K-theory PBL parameterization following Keyser and Anthes (1982, denoted KA82).

2. Boundary Layer Formulation

The boundary layer parameterization employed KA82, which is based on the high-resolution nocturnal PBL parameterization of Blackadar (1978). Turbulent fluxes are represented in K theory by

$$\overline{u'w'} = -K_{mz}\frac{\partial u}{\partial z},$$

The diffusion coefficient Kmz is calculated implicitly from model shear and stability fields to minimize a priori assumptions about the boundary layer structure. The coefficients are broken down into a small, constant diffusive part Kz0 and a variable part:

$$K_{mz} = K_{\theta z} = \begin{cases} K_{z0} + k_0^2 l^2 S \left(\dfrac{\mathrm{Ri}_c - \mathrm{Ri}}{\mathrm{Ri}_c} \right), & \mathrm{Ri} < \mathrm{Ri}_c \\ K_{z0}, & \mathrm{Ri} \geq \mathrm{Ri}_c \end{cases}$$

where k_0 is the von Karman constant, and the critical Richardson number Ric = 0.25 (Blackadar, 1978). Note that the vertical shear dependence is included in Ri. The fourth-order diffusion coefficients are defined following KA82 as

$$K_H = (\Delta x)^2 \left\{ K_{H0} + \frac{1}{2} k_0^2 (\Delta x)^2 \left[\left(\frac{\partial u}{\partial x} \right)^2 + \left(\frac{\partial v}{\partial x} \right)^2 \right]^{1/2} \right\}.$$

Vertical and horizontal diffusion coefficients for the momentum and mass fields are given equal values within each model. Finite differencing tends to give systematically greater values of Ri than the mean Ri within the layer (Blackadar, 1978), so Ric = 1.0 vice the theoretical value of 0.25 to account for the finite grid resolution (following KA82). The surface layer fluxes are modelled after Monin-Obukov similarity theory.

The model domain extends 3600 km in the east-west (x) direction and 12 km vertically. Horizontal grid spacing is 40 km and there are 50 vertical levels uniformly spaced in z, corresponding to 240 m spacing over flat topography. The time increment is 90 s. The surface topography is defined by

$$z_s = h \cos^2 \left[\frac{\pi (x - W/2)}{\epsilon W} \right], \quad |x - W/2| \leq \frac{\epsilon W}{2}.$$

The mountain height h is held constant while the width e (the fraction of the horizontal domain occupied by the mountain) is varied between 0.6 and 0.2. Fourth-order diffusion constants in the inviscid model are given the value K0 at the surface and increase linearly in the vertical to a factor of 10 at the upper boundary. A hyperbolic sponge layer is also included near the top of the domain.

Initial fields are the same as those used in W92. The non-frontal mountain initial flow is defined by semigeostrophic solutions (following Merkine, 1975). In frontal simulations, a perturbation is added to these basic fields. Initial u, v and w fields are derived using the thermal wind, quasigeostrophic circulation, and continuity equations.

3. Numerical Solutions

a) Frontal solutions with no topography

The model is run first with no topography to serve as a control case for the mountain simulations. Figure 1 contains the frontal solutions after 48 hours of integration. Only the lower part of the atmosphere is shown to highlight near-surface effects. The front has intensified and all fields have been advected downstream with the background current.

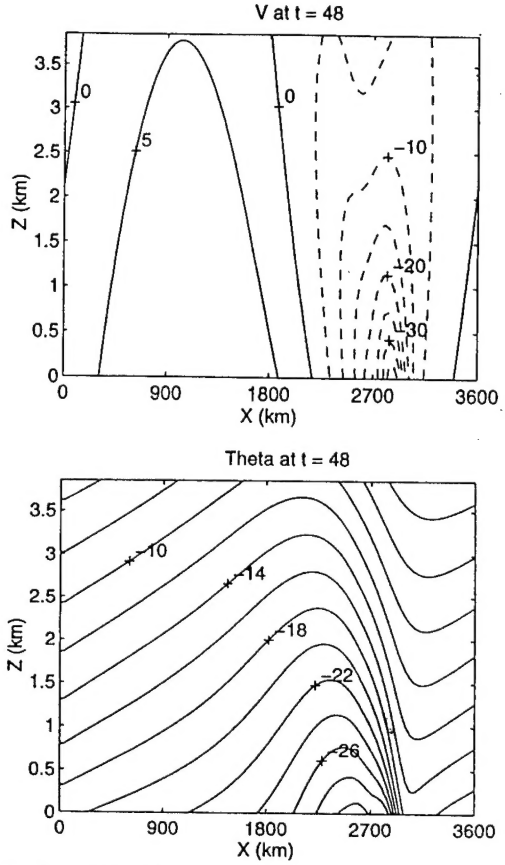

Figure 1. (a) Along-front wind component and (b) potential temperature for inviscid front at t = 48h.

These fields clearly show the maximum thermal gradient and associated vorticity maxima at the surface, decreasing rapidly with height. The corresponding PBL solutions are shown in Fig. 2. Strong vertical mixing is evident in the near-vertical potential temperature contours throughout the 1.0 to 1.2 km well-mixed layer. The frontal zone is weaker than that shown in Fig. 1, and the thermal gradient is constant throughout the PBL. Here the cross-front and along-front wind maxima are elevated jets near the top of the PBL as winds are frictionally forced to zero at the surface. A major finding here is that the simulated fronts are always weaker when PBL effects are included, due primarily to vertical mixing. The turbulent mixing of the weaker-gradient upper PBL air reduces the potential temperature gradient at the surface.

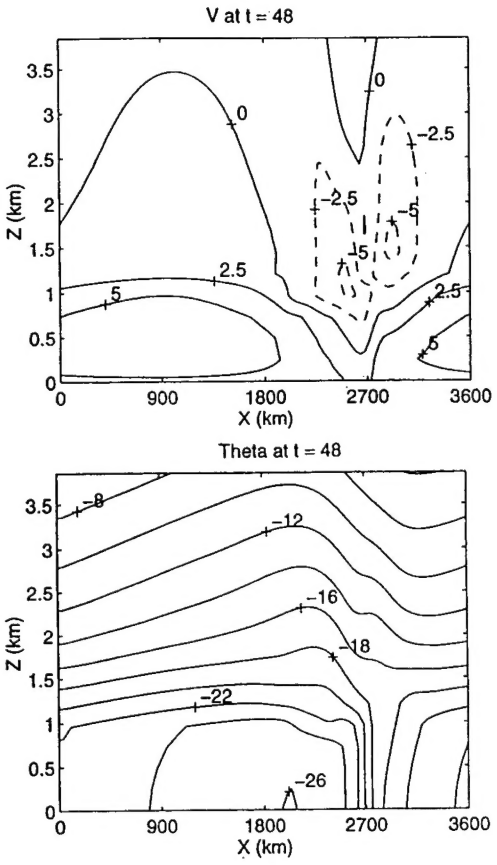

Figure 2. Same as in Fig. 1 except with PBL.

To quantify the strength of the frontal zone, the parameter d is defined as

$$d = \frac{|\Delta\theta|}{\left|\frac{\partial\theta}{\partial x}\right|_{max}},$$

where $\Delta\theta$ is the maximum horizontal potential temperature variation on the lowest numerical level. The temporal evolution of the d-value for the flat topography simulations is shown in Figure 3. After an initial period of reduced frontogenesis, the PBL front undergoes frontogenesis at a rate nearly equal to that of the inviscid front (indicated by the slopes of the curves in Figure 3) until about 36 h, when it reaches maximum intensity. At this point the frontogenetical forcing is matched by the diffusive forcing and the front is in steady-state.

The front in the PBL case also translates slower than the frictionless front, which is over 200 km further downstream at t = 48 h. The increase in the distance that the PBL front lags behind is correlated to the difference in maximum cross-frontal velocities (figures not shown). It appears that the reduction of the cross-frontal wind velocity caused by the PBL results in a slower translation speed and a different vertical tilt.

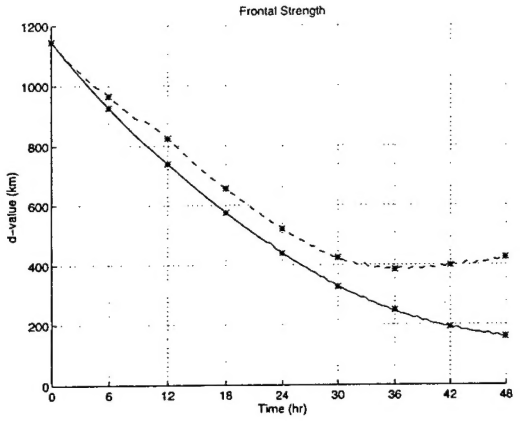

Figure 3. Frontal strength measured by the d-value for the inviscid case (solid line) and PBL case (dashed line).

b) Non-frontal solutions with topography

Before investigating topographic effects on the fronts, the effects of the PBL on the basic flow over the ridge must be examined. For the e = 0.6 ridge, the t = 48 h fields show only a slight departure from the semigeostrophic solutions as weak wave activity is generated and the cross-ridge velocity maximum shifts slightly toward the lee slope. The PBL solutions for t = 48 h (Fig. 4) are more asymmetrical in the lower layers in this respect as the elevated cross-frontal jet is displaced significantly over the lee slope. No gravity waves are evident in the figure, however. The e = 0.4 ridge produces similar t = 48 h solutions, but with stronger mountain-forced wind fields and larger amplitude gravity waves, which begin to appear in the PBL case. The e = 0.2 mountain inviscid solution exhibits a dramatic departure from the semigeostrophic solution. As the mountain slope becomes steeper, the cross-mountain flow is accelerated more strongly and advected over the lee slope. In the inviscid simulations, the maximum winds are at the surface and an evident hydraulic jump is generated when the high speed winds reach the base of the slope. This causes the well-mixed area at the base of the lee slope and the flow reversal above the lee slope u and v maxima. Large amplitude, upward propagating gravity waves also result from the hydraulic jump (W92). In contrast, the PBL solution at t = 48 h (Fig. 5) shows no such abrupt effects. Lee slope winds are enhanced, creating gravity waves, but the elevated jet is "insulated" from the topography by the PBL, so the topographic slope changes do not force the abrupt changes in momentum exhibited in the inviscid simulation.

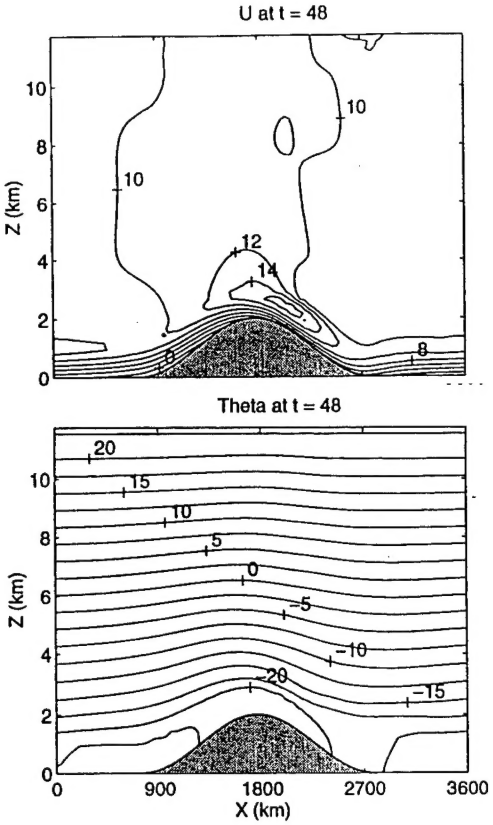

Figure 4. Mountain solution for e = 0.6 profile at t = 48 h with PBL.

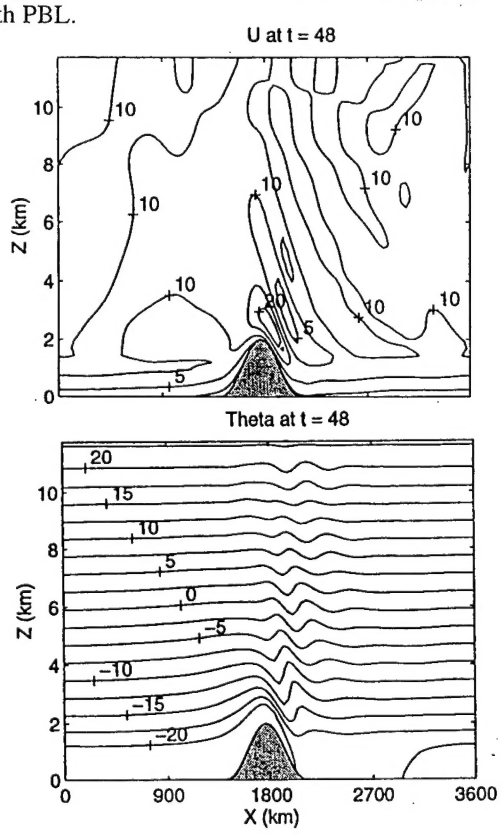

Figure 5. Same as in Fig. 4 except for e = 0.2 mountain profile.

In order to investigate the dynamical effects of the mountain-forced circulations on frontogenesis, the divergence fields are examined. The divergence fields of the e= 0.6 mountain solutions at t = 24 h are shown in Fig. 6. The mountain circulations are well-developed by 24 h, and this roughly corresponds to the time that the fronts cross the ridge in the frontal simulations. In the inviscid case (Fig. 6a), the flow is divergent on the upwind slope as the air accelerates over the ridge. Strong convergence is shown on the lee slope, caused by the rapid decrease in velocity downstream of the cross-ridge jet velocity maximum. The horizontal divergence field is complicated in the PBL case (Fig. 6b) because the wind decreases to zero at the surface, producing significant convergence in the PBL on the upwind slope overridden by a divergent area as the winds above the PBL accelerate over the ridge. Conversely, the lee slope is characterized by divergence within the PBL overridden by an area of convergence. There is less convergence on the lee slope in the PBL case because the winds do not decrease so rapidly near the base. The weaker elevated jet does not enhance the lee side convergence surface as much as in the frictionless case.

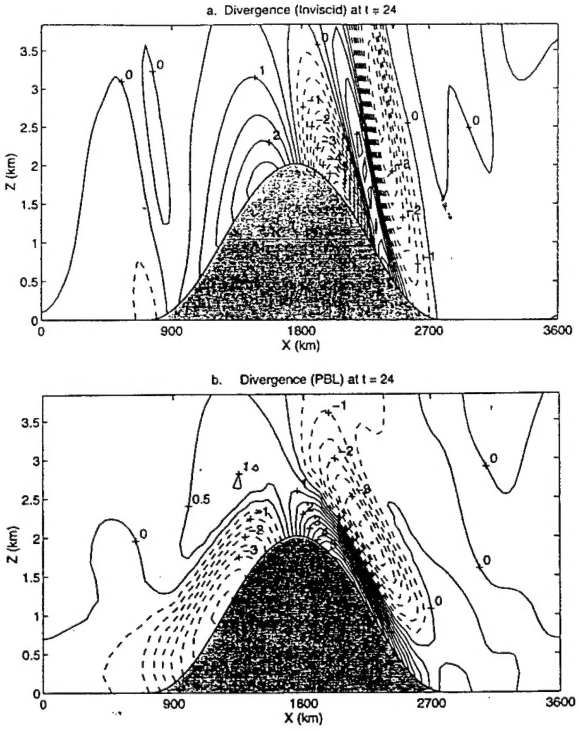

Figure 6. Divergence field at t = 24 h for; a) the inviscid mountain and b) the mountain with PBL.

The boundary layer also forces a horizontal temperature gradient within the PBL due to vertical mixing on the mountain slope. Vertical mixing reaches a higher potential temperature level near the top of the ridge than near the

base because the stability increases over the ridge. The PBL is therefore mixed with air at a higher potential temperature near the top of the ridge. This produces a positive temperature gradient on the upwind slope and a negative temperature gradient on the lee slope, as shown in Fig. 7 at t = 24 h. The thermal pattern advects downstream somewhat, but is nearly at steady-state by t = 24 h. The effect is unique to the mountain PBL cases because mixing to differing é-levels is required to produce a horizontal temperature gradient. The strength of the gradient produced is also highly dependent on the vertical thermal structure, as will be demonstrated in the frontal simulations.

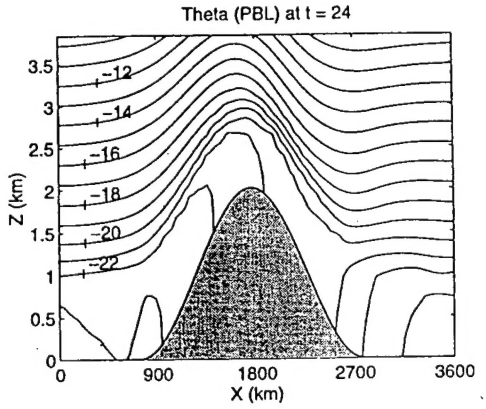

Figure 7. Potential temperature for mountain with PBL at t = 24 h.

c) Frontal solutions with topography

In these simulations, the frontal forcing is applied to the model over the mountain domain. Fig. 8 contains the time evolution of the potential temperature field at 6 h intervals for both the inviscid and PBL frontal simulations over the e = 0.6 mountain. By t = 6 h, a well-mixed layer is already developed in the PBL case. The vertical mixing has produced a significant strengthening of the surface potential temperature gradient compared to the frictionless potential temperature field. Here the mixing has a greater effect in the thermal gradient than in the non-frontal case because the initial temperature perturbation increases the differential potential temperature level mixing effect described in the previous section. The trend continues through t = 12 h (Fig. 8a) as the well-mixed layer continues to develop and deepen.

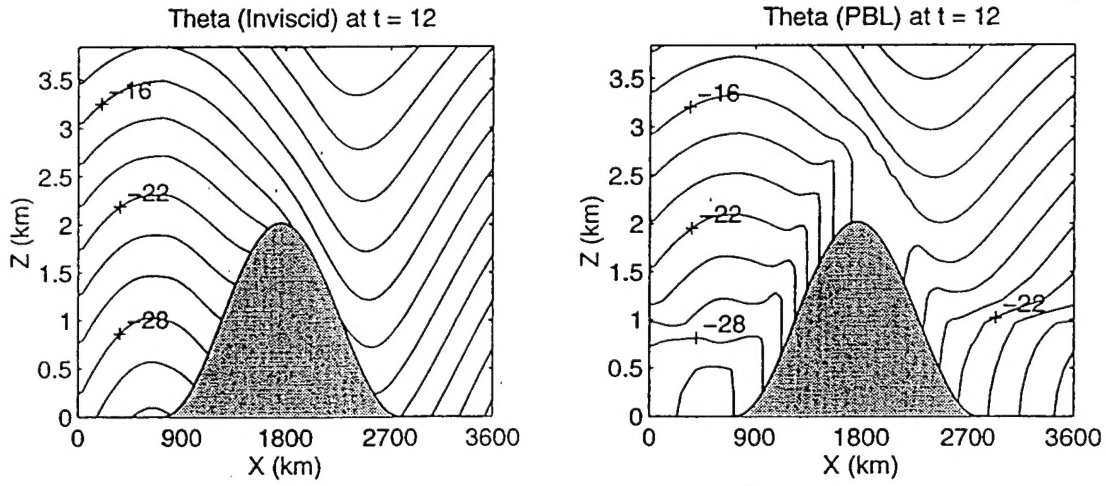

Figure 8. Frontal evolutions over mountain at 12 h interval. The left panels are for the inviscid case and the right panels are for the case with PBL.

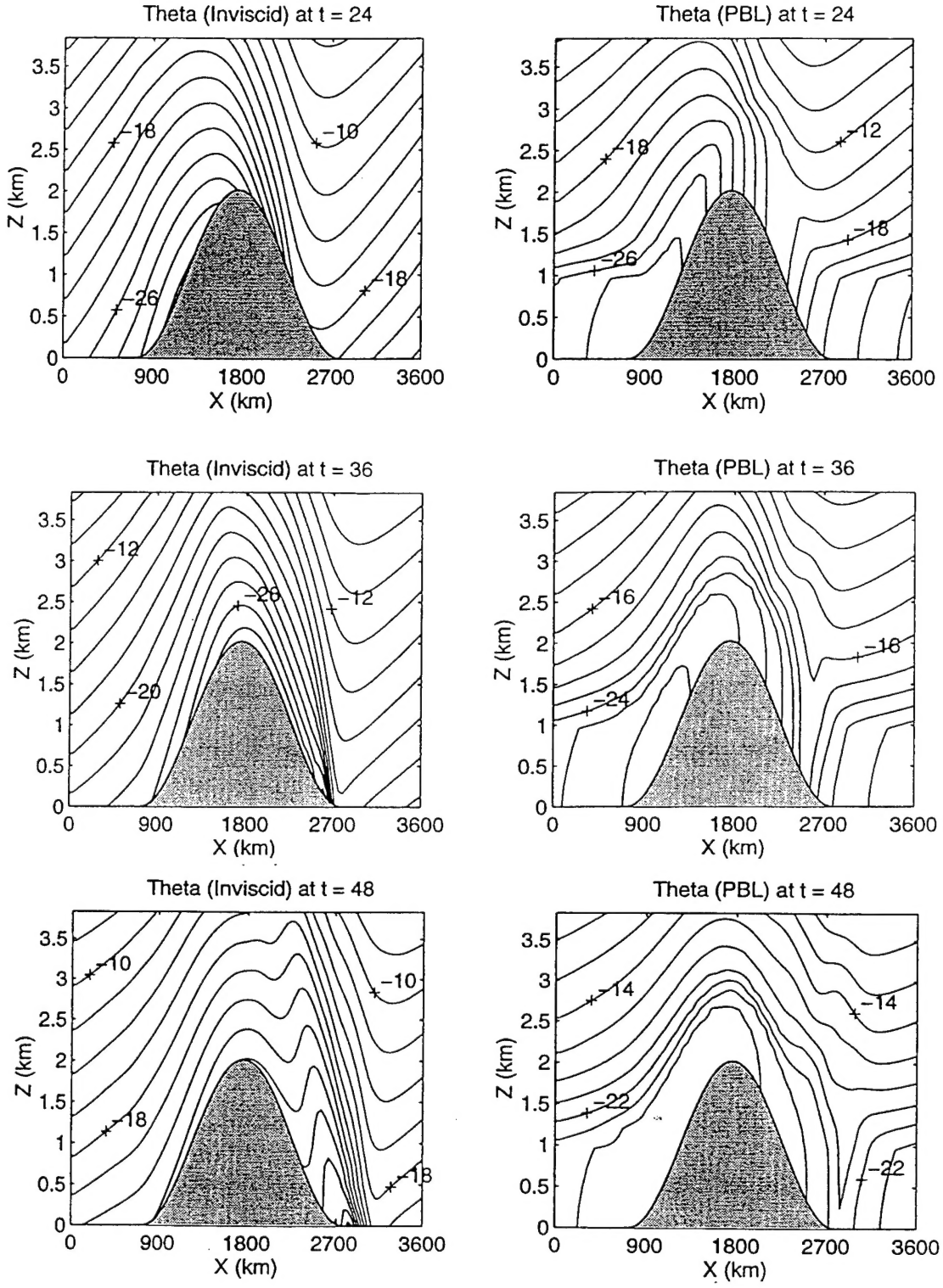

Figure 8. Continued.

At about t = 24 hr, the inviscid front reaches the crest of the ridge and moves down the lee slope in the next 18 h, undergoing rapid frontogenesis. The PBL front lags behind by about 12 h, and increases in intensity at a much lower rate as it reaches the lee slope (Figure 8d-f) and then gradually weakens on the lower half of the lee slope. Conversely, the inviscid front continues to strengthen over the entire lee slope and weakens slightly as it reaches the downwind plane at t = 48 h. By the end of the simulation at t = 48 h, the PBL front is much less intense than the inviscid front. The frontal strength variations are summarized for the $\hat{\imath}$ = 0.6 mountain in Fig. 9, which contains the temporal evolution of the d-values for both frictionless and PBL simulations. The flat topography frontal solutions are included in the figure for reference. The corresponding six-hourly frontal positions are shown in Figure 10. The d-values show that in the frictionless case, the front weakens significantly on the upper half of the upwind slope and then undergoes strong frontogenesis on the lee slope. This is the same effect observed in W92, attributed to the mountain-forced divergence field. The weakening near t = 48 h is also observed in W92 and is shown to be caused by a small area of divergence at the base of the lee slope. The PBL d-value curve confirms that the PBL front is stronger on the upwind slope and weaker on the lee slope compared to the frictionless case.

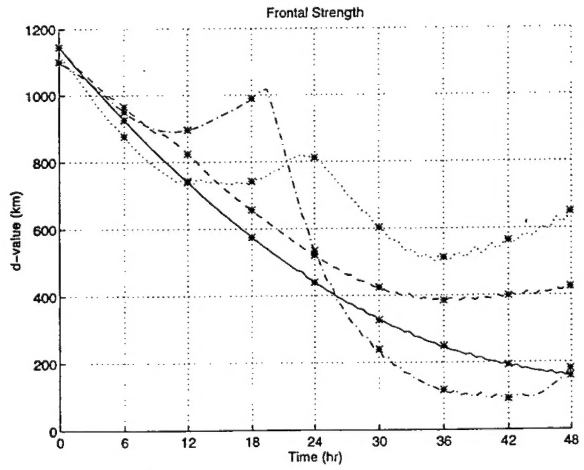

Figure 9. Frontal strength measured by the d-value for fronts over inviscid mountain (dash-dotted line) and mountain with PBL (dotted line). Curves for flat-topography cases shown in Fig. 3 are also included for comparison.

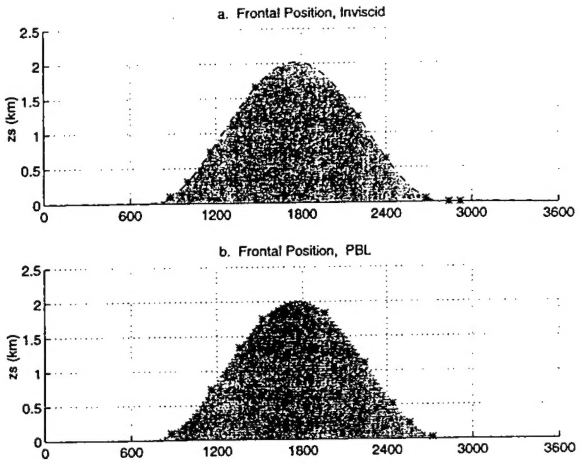

Figure 10. Frontal positions corresponding to the mountain cases in Fig. 9.

Comparison of the d-value curves to those of the flat topography simulations reveals several interesting features. In the flat topography cases, the PBL front is weaker than the inviscid front at all times. Note also that the inviscid front is weaker in the mountain case than in the flat topography case even on the lower half of the upwind slope (before the period of frontolysis). The mountain PBL front, however, is stronger than both the inviscid mountain front and the flat topography PBL front for the first 12 h of the simulation. Thus the combination of the mountainous topography and the PBL has a frontogenetical effect on the upwind slope. The overall effect opposes this upwind slope effect, however. The final strength of the fronts in the frictionless simulations are similar whether or not topography is included (confirmed in W92 by extending the integration to t = 60 h). In the PBL simulations, however, the front is significantly weaker in the mountain case at t = 48 h. In contrast to the inviscid results, when PBL effects are included, the mountain appears to have a net frontolytical effect.

The e = 0.4 and 0.2 mountain simulation produces similar trends

4. Summary

The numerical simulations contained in this study demonstrate that the PBL plays an important role in frontal dynamics over mountainous topography. In the mountain simulations, the elevation of the cross-ridge jet to the top of the PBL greatly reduces gravity wave generation and eliminates hydraulic jump effects in the mountain profiles considered. These results are more realistic than those of the W92 inviscid study, which generates more wave activity than is realistic for smooth, synoptic-scale ridges. The weaker elevated jet also results in much weaker lee slope

convergence, which is the dominant forcing mechanism in the inviscid study. Turbulent mixing on the mountain slopes is shown to indirectly affect frontal dynamics. The PBL reaches higher é-levels on the ridge than on the adjacent planes, producing a horizontal temperature gradient in the well-mixed layer. This gradient has a large effect on frontal forcing because the convergence terms are proportional to the horizontal temperature gradient.

In summary, the front still shows frontolysis on the upwind slope and increased frontogenesis on the lee slope when PBL effects are included, but the magnitude of the variation is less than in the inviscid simulations. On the upwind slope, frictional convergence in the PBL due to the mountain slope combines with the mixing-enhanced horizontal temperature gradient. This produces a stronger front on the upwind slope and partially counteracts the weakening caused by the divergence associated with the accelerating cross-mountain flow above the PBL. On the lee slope, convergence forcing is quite small or even negative in the PBL simulations because of reduced convergence associated with the cross-ridge jet and frictional divergence in the PBL near the surface. The result is that the PBL front intensifies much more slowly than in the inviscid case and begins to weaken over the lower half of the lee slope. In contrast to the inviscid simulations, the net effect of the front passing over the mountain is frontolytical when PBL effects are included. Narrower mountain profiles produce slightly different results because the fronts begin forming further upstream relative to the mountain, but the results are consistent over the ridge itself.

The study demonstrates the importance of the lower atmosphere in mountain dynamics. The vertical mixing of the PBL on sloping terrain produces unique effects and it is clear that the inclusion of a realistic PBL parameterization is even more critical in these frontogenesis simulations than in their flat topography counterparts.

Acknowledgments. This study was in part supported by the National Science Foundation Division of Atmospheric Science under Grant ATM-9208751.

REFERENCES

Blackadar, A. K., 1978: High-resolution models of the planetary boundary layer. Advances in Environmental Science and Engineering, Vol. 1, J. R. Pfafflin and E. N. Ziegler, Eds., Gordon and Breach, 50-85.

Dunst, M., and A. Rhodin, 1990: On the influence of frictional effects on surface fronts. Beitr. Phys. Atmos., 63, 223-242.

Hartsough, C. S., and W. Blumen, 1990: Objective cross-sectional analysis of diabatic circulation and vertical motions using ALPEX data. Meteorol. Atmos. Phys., 43, 221-230.

Keyser, D., and R. A. Anthes, 1982: The influence of planetary boundary layer physics on frontal structure in the Hoskins-Bretherton horizontal shear model. J. Atmos. Sci., 39, 1783-1802.

Merkine, L.-O., 1975: Steady finite-amplitude baroclinic flows over long topography in a rotating stratified atmosphere. J. Atmos. Sci., 32, 1881-1893.

Radinovic, D., 1986: Analysis of ALPEX data, 20, 21 March and 24, 25, 30 April 1982. PSMP Report Series 22, WMO/TD No 154.

Williams, R. T., M. S. Peng, and D. A. Zankofski, 1992: Effects of topography on fronts. J. Atmos. Sci., 49, 287-305.